SoRo
Soft Robotics

ORIGINAL ARTICLE

Soft, Rotating Pneumatic Actuator

Alar Ainla,[1,*] Mohit S. Verma,[1,*] Dian Yang,[2,*] and George M. Whitesides[1,3,4]

Abstract

This article describes a soft pneumatic actuator that generates cyclical motion. The actuator consists of several (three, four, or five) chambers (arranged around the circumference of a circle surrounding a central rod) that can be actuated independently using negative pressure (or partial vacuum). Sequential actuation of the four-chamber device using reduced pressure moves the central rod cyclically in an approximately square path. We characterize the trajectory of the actuator and the force exerted by it, as we vary the material used for fabrication, the number of chambers, and the size of the actuator. We demonstrate two applications of this actuator: to deliver fluid while stirring (by replacing the central rod with a needle) and for locomotion that mimics a reptilian gait (by combining four actuators together).

Keywords: cyclic, locomotion, buckling, vacuum, stirrer, biomimetic

Introduction

S OFT AND HARD ACTUATORS—as they are developing—seem to have different and complementary capabilities.[1–19] Hard actuators, for example, are superior when high force, accuracy of positioning, repeatability, and speed of actuation are required. Soft actuators are more directly compatible with tasks requiring delicacy, adaptability, collaborativity (meaning the ability to operate safely with humans), resistance to damage by impact, and light weight.[1–6,20,21] That complementarity in characteristics is not exclusive, and there are types of motion required by both soft and hard systems: one of these is what we will call "cyclical" motions.

Cyclical motion in a circular trajectory is very easily accomplished in hard systems using a wheel or ring, an axel, and bearings that allow motion of the axel relative to the bearing: the wheels in automobiles or the hands in an analog clock are examples. For soft systems, the design generating an analogous function is not immediately obvious. What would be a corresponding system—one capable of pointing in any direction relative to a central axis—for a device that does not have a wheel, axel, or bearings? There are a number of possible solutions for this problem. Here, we describe one, based on a circular array of pneumatically actuated

subcomponents—which we call a cyclical vacuum-actuated machine (cVAM, Fig. 1). Mazzeo and colleagues have recently described a system that is related in concept, although different in execution and application.[22]

Prior work[4,22–29] on soft actuators has suggested a number of approaches related to what we describe here. Wait *et al.* developed a spherical rolling robot using inflatable rubber bladders.[23] Rus and colleagues demonstrated the coordinated use of pairs of soft bending actuators to achieve rolling motion.[24] Mazzolai *et al.* demonstrated the use of shape memory alloys to mimic tentacles of octopus.[25] We demonstrated pneumatic tentacles capable of pointing in any direction in the plane of their base (and by extension of the principle on which they operate) in directions spanning more than 90° from the perpendicular to that plane.[4] We also demonstrated (in the course of research focused more in fabrication than in actuation) structures ("click-e-bricks") capable of limited directional pointing.[28] Rus and colleagues made a soft pneumatic belt that can roll by sequential actuation of the actuators arranged in a ring.[26] Lazarus and Reis used an auxetic design to achieve bending and twisting in a cylindrical actuator.[29] Mazzeo and colleagues demonstrated that sequential inflation of actuators positioned around the circumference of a circle can produce rotational motion; they thus created soft wheels.[22]

[1]Department of Chemistry and Chemical Biology, Harvard University, Cambridge, Massachusetts.
[2]School of Engineering and Applied Sciences, Harvard University, Cambridge, Massachusetts.
[3]Wyss Institute for Biologically Inspired Engineering, Harvard University, Cambridge, Massachusetts.
[4]Kavli Institute for Bionano Science and Technology, Harvard University, Cambridge, Massachusetts.
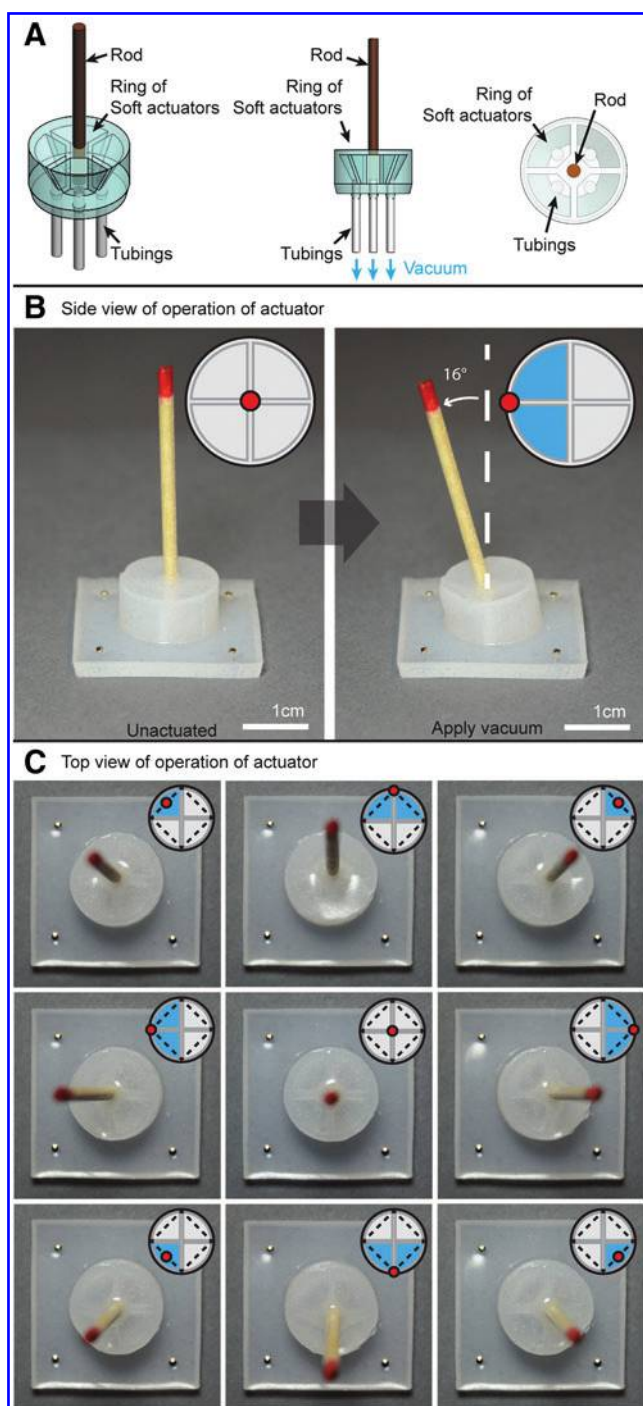*These authors contributed equally.

FIG. 1. **(A)** Schematics showing the design of a cVAM. A typical cVAM unit contains four soft pneumatic air chambers that can pull the central hard rod in different directions upon application of vacuum. **(B)** Images of a cVAM unit where the left two neighboring chambers are actuated at the same time by applying a negative pressure of −90 kPa (marked by *blue shading* in the schematic), tilting the rod (shown as a *red circle* in the schematic) in the middle. The tubing is fed through a hole on the gray platform, which is covered by the actuator and hidden from view. Scale bars are 1 cm. **(C)** Eight distinct directions are achieved by applying vacuum to one or two neighboring air chambers. A neutral position is shown in the middle when no vacuum is applied. cVAM, cyclical vacuum-actuated machine.

TABLE 1. COMPARISON OF THE ROTARY ACTUATOR
DEVELOPED BY MAZZEO *ET AL.*
AND OUR CYCLICAL VACUUM-ACTUATED MACHINE

Property	Mazzeo's Rotary actuator[22]	Current work cVAMs
Actuation type	Rotation	Angular deflection and revolution
Pneumatic source	Pressure ($\sim$50 to 100 kPa)	Vacuum (−5 to −90 kPa)
Degrees of freedom	1 (angle)	2 (angle, radius)
Drive mode	Digital	Digital or analog
Construction	2 parts (stator and rotor)	1 part (monolithic)
Analogy	Stepper motor	Joystick
Number of compartments	16	3, 4, or 5
Number of independent pneumatic inputs	4	3, 4, or 5
Number of steps in one full rotation or revolution	16	3, 4, 5, or 6, 8, 10
Frequency range	$\sim$14–18 rpm	$\sim$10–1000 rpm
Power output	8.4 or 26 mW	2.3 mW
Thermodynamic efficiency	Not reported	$\sim$2%
Lifetime	Not reported	>10^6 cycles

cVAM, cyclical vacuum-actuated machine.

The structure shown in Figure 1 follows principles related to the pneumatic wheel of Mazzeo *et al.*, but has three key differences. (1) A cVAM acts as a single part (because the central rod and the surrounding chambers are joined). Mazzeo's rotary actuator has two parts—a stator and a rotor. (2) A cVAM uses negative pressure (vacuum) as the pneumatic source of power, as opposed to positive pressure; it thus has no risk of bursting from overpressure, and also a different relationship between power output and size/structure. (3) A cVAM is analogous to a joystick, whereas Mazzeo's rotary actuator is similar to a stepper motor. The joystick design allows more degrees of freedom in actuation than a stepper motor, but also places greater demands on the part of the structure where "revolution" (perhaps better described in cVAMs as "flexing" or "wobbling") occurs. Other technical differences are summarized in Table 1.

Results and Discussion

Schematics and operation of cVAM

A cVAM consists of four soft pneumatic chambers organized in a ring; these surround and steer a central rod whose top moves approximately in a two-dimensional plane (Fig. 1 and Supplementary Movie S1; Supplementary Data are available online at www.liebertpub.com/soro). The cVAM is fabricated by molding elastomers (using three-dimensional-printed parts) and positioning a rigid rod (in Fig. 1, a wooden dowel) in the center of the device by curing the elastomer around its base (Supplementary Fig. S1). When a differential pressure of −90 kPa (partial vacuum inside the chambers) is applied to two adjacent chambers, the rod deflects from the vertical by $\sim$16° (Fig. 1B). Figure 1C illustrates various positions that can be attained by the rod by sequential actuation of adjacent chambers.

Characterizing the torque obtained from cVAMs

We fabricated cVAMs using elastomers (Supplementary Table S1) with different values of stiffness (as characterized by their elastic modulus) and characterized their actuation with and without load using the setup illustrated in Figure 2A,
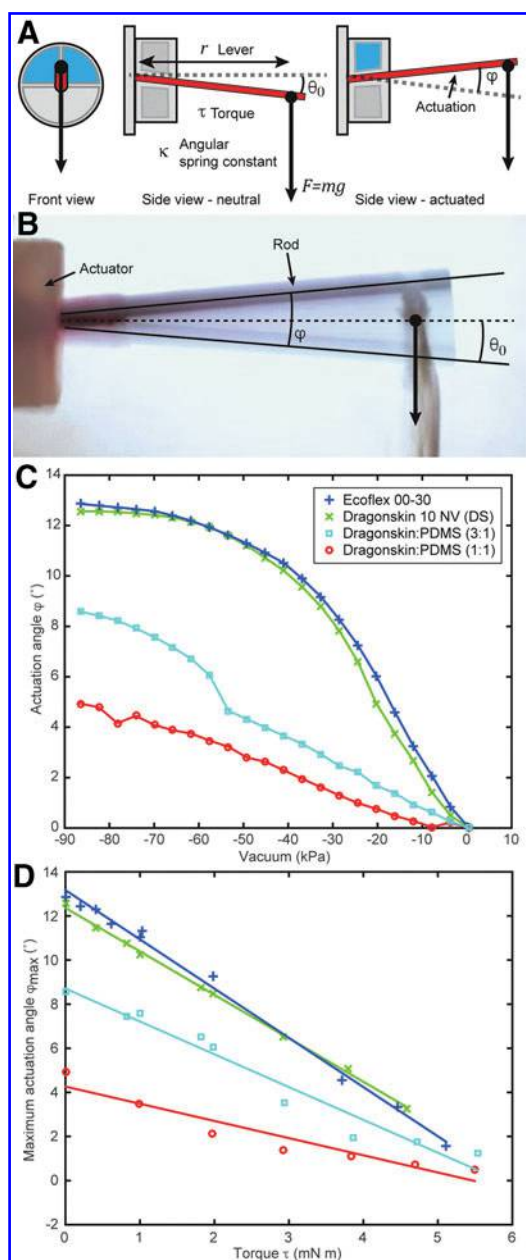
FIG. 2. The effect of materials used for fabricating the actuators (all actuators are of the same size and have four chambers). **(A)** Schematic of the setup used for characterization: two chambers (*highlighted with blue shading*) were actuated and the actuator was used to lift weight. The negative pressure (relative to atmosphere) was ramped continuously with an electronic pressure control system as described in the supplementary information. The actuation angle φ was recorded using a camera from the side. **(B)** Time-averaged actuation as seen from the side. **(C)** Actuation angle as a function of applied negative pressure for actuators made of different materials (no load was applied, $\tau = 0$). Initial slopes (in the linear regime at relatively small actuation angles) are $\sim 0.28°$/kPa, $\sim 0.09°$/kPa, and $\sim 0.06°$/kPa, respectively. **(D)** Maximum actuation φ_{max} as a function of different loads (varying torque). The maximum actuation decreases with increased load but the effect is less severe for stiffer elastomers (they have smaller slope). Further characterization is provided in supplementary information.

where we evacuate two of the four chambers to move the central rod against gravity. Figure 2B shows a time-averaged image obtained for a typical actuator (as observed from a side view) with a load at the tip of the rod. The pressure difference between the inside and outside of the chambers was varied using a custom-built electronic pressure regulator (see Supplementary Data, Supplementary Table S6 and Fig. S8 for details on assembly and operation) over the range of 0 to −90 kPa in increments of ~ 4 kPa to obtain Figure 2C. As expected, actuators fabricated in stiffer elastomers show a smaller deflection of the rod at the same negative pressure. The actuator fabricated in 1:1 v/v mixture of Dragonskin:PDMS does not actuate completely under atmospheric conditions because the pressure difference is limited, but it could be useful for hyperbaric applications (such as deep-sea exploration).

When a load is added to the tip of the rod, Figure 2D shows the maximum angle of actuation (as illustrated in Fig. 2A; sometimes, failure is possible as seen in Supplementary Fig. S10) for actuators fabricated in different elastomers (when evacuated at −90 kPa). The slopes of the lines in this plot (Supplementary Tables S2 and S7) confirm that stiffer elastomers are less affected by the addition of load than softer elastomers. The deflection of the rod without applied negative pressure and the work done by the actuators are presented in Supplementary Figure S3.

Scaling the size (by $2\times$ or $3\times$) of the actuator shows the expected trends in its performance as indicated in Supplementary Figure S4 and explained in the Analysis section of Supplementary Data.

Dynamic characterization of cVAM

We also characterized the dependence of the angle of deflection (i.e., the angle between the initial position of the rod and its position upon actuation) of the rod on the frequency of revolution (number of revolutions per minute, or rpm, where one revolution is completed when the tip of the rod follows a trajectory that returns it to its initial position). By tracking the trajectory of the tip of the rod (see Supplementary Movie S3 for a typical video used for characterization), Figure 3 illustrates that the rod follows a trajectory whose shape is governed by the number of chambers (i.e., it will form a triangle, a square, or a pentagon, for three, four, or five chambers, respectively). One revolution involves 6, 8, or 10 steps for 3, 4, or 5 chambers as illustrated in Figure 3A.

The frequency of revolution (See Supplementary Data, Supplementary Fig. S9, and Table S4 for details on the contributions of different components of the system to the time needed for actuation) is controlled by changing how long the rod is held at each of these steps (we will refer to this time as hold time). When two adjacent chambers of the cVAM are actuated, the rod is at the corner of its respective shape; actuating a single chamber brings the rod approximately halfway around the edge of its respective shape. The shape of the trajectory is relatively constant as the hold time changes from 200 to 50 ms (Fig. 3A) and the maximum angle of deflection (Fig. 3B) decreases more severely ($\sim 0.005°$/rpm) for three- and four-chamber actuators than for the five-chamber actuator ($\sim 0.001°$/rpm). As we increase the frequency of revolution further (hold time of 5 ms), the trajectory starts to become more circular (Fig. 3A).
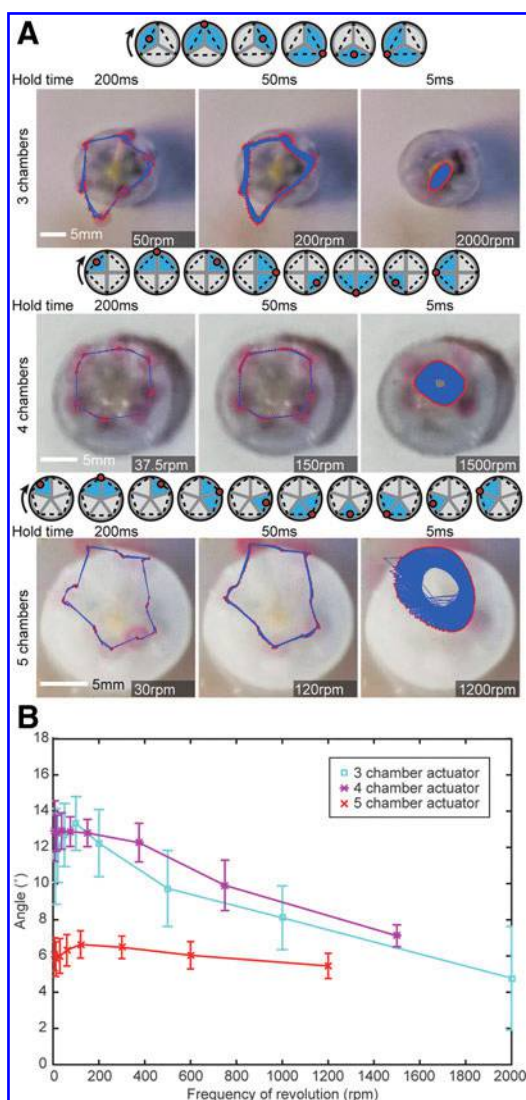
FIG. 3. The effect of varying the number of chambers (three, four, or five) on the actuation of cVAMs. All actuators are made of the same material (Ecoflex 00–30) and are of the same size. Volume of each chamber is 137, 99, and 75 μL for actuators with three, four, and five chambers, respectively. **(A)** Schematic representation of the order of actuation of the chambers (6, 8, or 10 steps per revolution), *blue* shows evacuated chambers, and *red circle* shows movement of tip position. Changes in the angle of deflection were obtained as a function of frequency of revolution (adjusted by changing the hold time at each step of the revolution). Images show three representative data points whereas the plot in part **(B)** represents maximum deflected angle for the entire range of frequencies of revolution that were tested. (The trajectory of the rod is slightly off-center because the camera was not perfectly aligned with the center of the rod.) A pressure difference between the chambers and the atmosphere of 90 kPa was used. The pictures presented here are time-averaged by overlaying frames from the corresponding video. The *red* marks show the location of the center of the rod as obtained from image tracking whereas *blue lines* indicate the trajectory. **(B)** Changes in the angle of deflection plotted as a function of the frequency of revolution. The values are reported as mean±SD obtained from the maximum deflection of the rod as the rod undergoes revolution at different frequencies (while being held at each frequency for 10 s and recorded in a video at 240 fps).
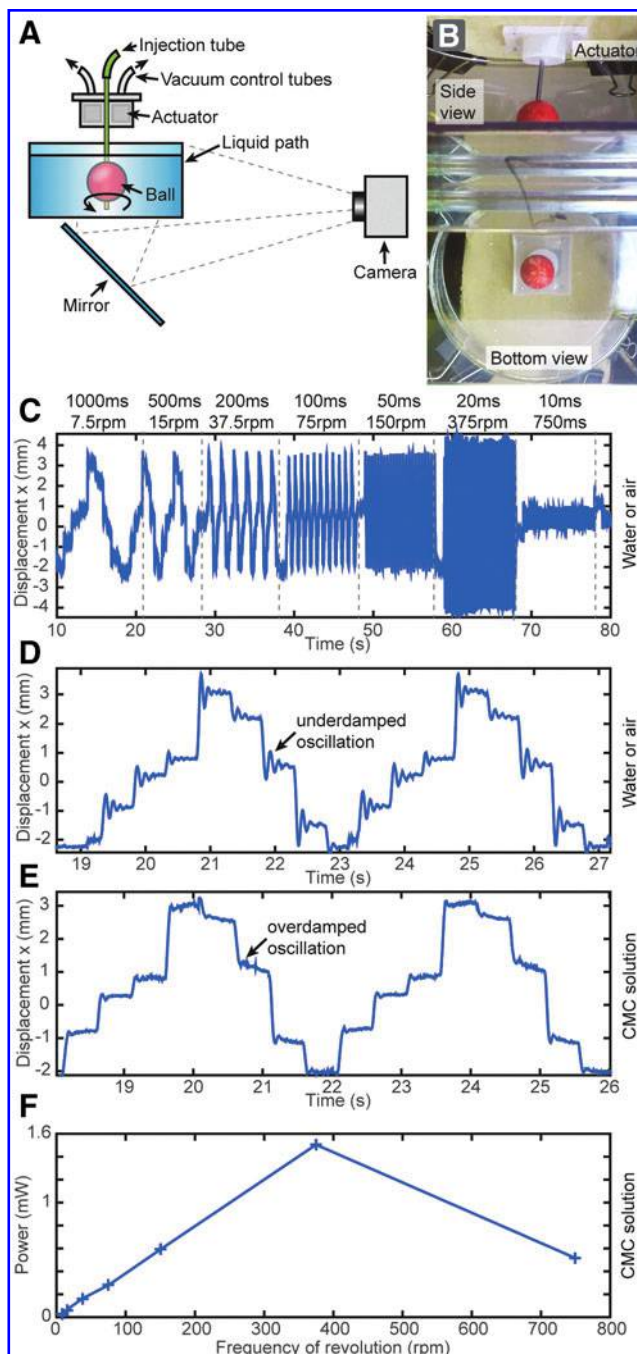

FIG. 4. Characterization of the cyclical actuation of cVAMs in fluids. **(A)** Schematic illustration of the experimental setup. **(B)** A sample image of the setup: the *bottom* view is obtained using a mirror placed at an angle. **(C)** Change in position of the ball as the frequency of revolution changes (by changing the hold time for each step of revolution; the hold time and frequency of revolution are shown above the plot). The oscillations are similar in air and water and also in the *x* and *y* directions because of symmetry. **(D, E)** Observations of underdamped oscillations (in water or air) and overdamped oscillations (in carboxymethylcellulose solution) during each step of the revolution. **(F)** Average power output of the cVAMs (calculated based on the estimates of work done by the rubber ball in viscous fluid) at different frequencies of revolution.
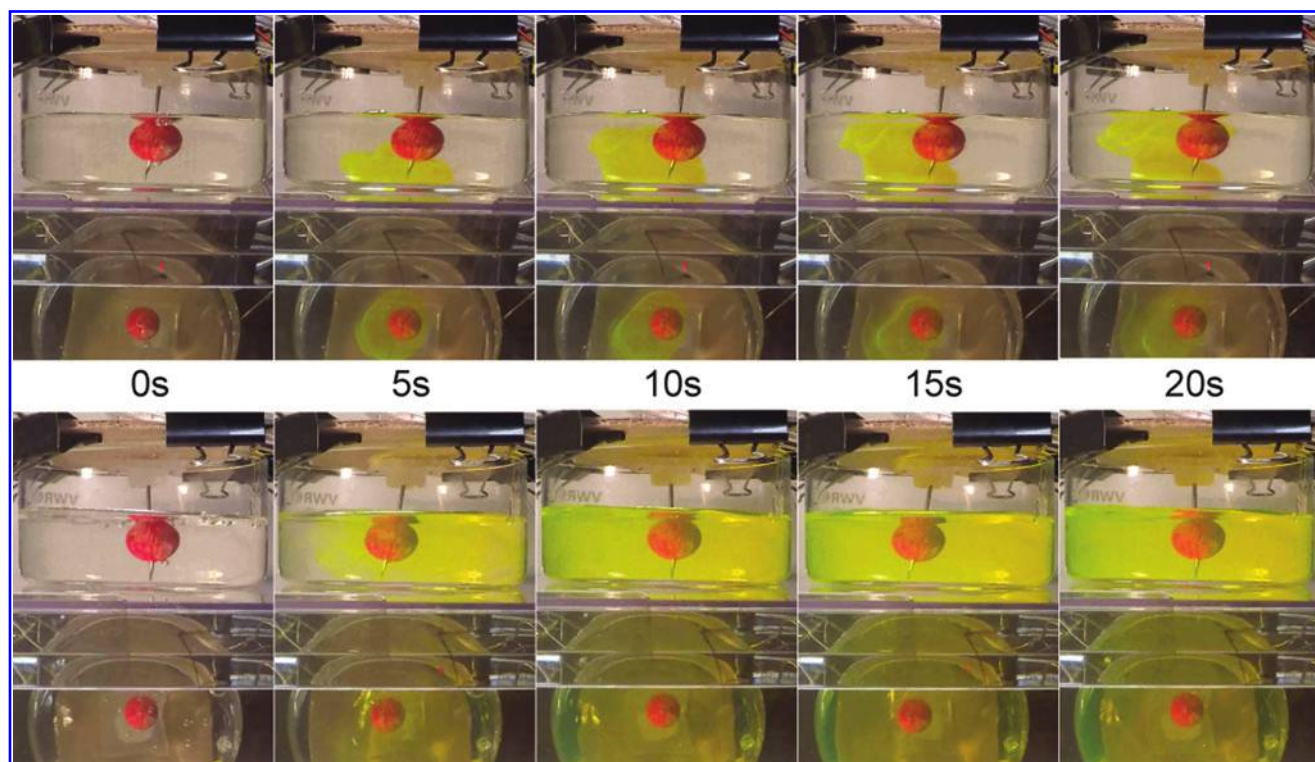
FIG. 5. Demonstration of simultaneous delivery of fluid and stirring using cVAM. A solution of fluorescein (1 mM in water) is delivered (at the rate of 10 mL/min) into a bath (150 mL) of water while the cVAM is off (*top sequence*) or operating at 375 rpm (*bottom sequence*). A video was captured (Supplementary Movie S5) and then frames were extracted at different time points. Each frame shows the *side* view and *bottom* view (reflected using a mirror at an angle).

While the actuator functions with different numbers of chambers, the four-chamber design provides the most consistent trajectory over a wide range of frequencies of operation (Fig. 3). Similar trends are observed when the actuator is scaled in size (Supplementary Fig. S5), but the larger actuator ($3 \times$ scaled) shows a more dramatic drop in the angle of deflection ($\sim 0.010°$/rpm) as a function of frequency of revolution.

When two chambers are actuated simultaneously, the angle of deflection is approximately twice that achieved by a single chamber (Supplementary Fig. S6 and Table S3) and the hysteresis is negligible as the negative pressure is ramped up or down (Supplementary Fig. S6 and Table S3).

Characterizing cyclical motion in a fluid

We used the actuator fabricated in Ecoflex 00–30 at $1 \times$ scale (Supplementary Fig. S1), with four chambers to characterize the cyclical motion in a fluid. Figure 4A shows a schematic of the setup used to characterize the motion of cVAMs in fluids. Three fluids with different viscosities were used to characterize it: air ($\eta \approx 0.02$ mPa·s), water ($\eta \approx 0.89$ mPa·s), 2% w/v carboxymethylcellulose ($\eta \approx 2300$ mPa·s) in water. Figure 4B shows sample images of the side view and bottom view of the stirrer. We operated the cVAMs at frequencies from 7.5 to 750 rpm by changing the hold time (ranging from 1000 to 10 ms) between each of the eight steps (Fig. 3A) that make up one complete revolution.

As expected, the cVAMs produce a periodic response (Fig. 4C), the frequency of revolution increases as the frequency of operation of its pneumatic valves (Supplementary Data, Fig. S7, and Table S5 provide details of the controller used for the valves) increases, while the amplitude of oscillation is approximately constant ($\pm 10\%$). At a frequency of revolution of 375 rpm (hold time of 20 ms), the amplitude of oscillation increases (by $\sim 60\%$), probably because the actuator is operating closer to resonance frequency. When the frequency of revolution is 750 rpm (hold time of 10 ms), the amplitude drops considerably (from ~ 4 to ~ 1 mm—a decrease of $\sim 80\%$). In comparison with the setup used in Figure 3, here we have added a load (a 2.4-g spherical rubber ball) to a needle (instead of a wooden dovel, such that fluid could be delivered or extracted as shown in Fig. 5) and thus, the response time (time between the signal from the solenoid valve and the movement of the ball) of the cVAM increases. Thus, a hold time of 10 ms is insufficient to achieve complete movement of the central rod.

We also observe that at the end of each of the eight steps of the revolution, the stirrer oscillates (with a decay) due to elasticity of the cVAMs (Fig. 4D). We can use these decaying oscillations to estimate the angular spring constant of the actuator as 0.0045 N·m·rad^{-1} and the angular damping constant because of the elastomer in air as 3.9×10^{-5} N·m·s·rad^{-1} (see details in Supplementary Data). The damping of the amplitude of this oscillation can be affected by the viscosity of the fluid, if the viscosity is high enough. For example, when the viscosity of the fluid is significantly higher (2300 mPa·s) than water (0.89 mPa·s), then the oscillator operates in an overdamped regime (Fig. 4E).
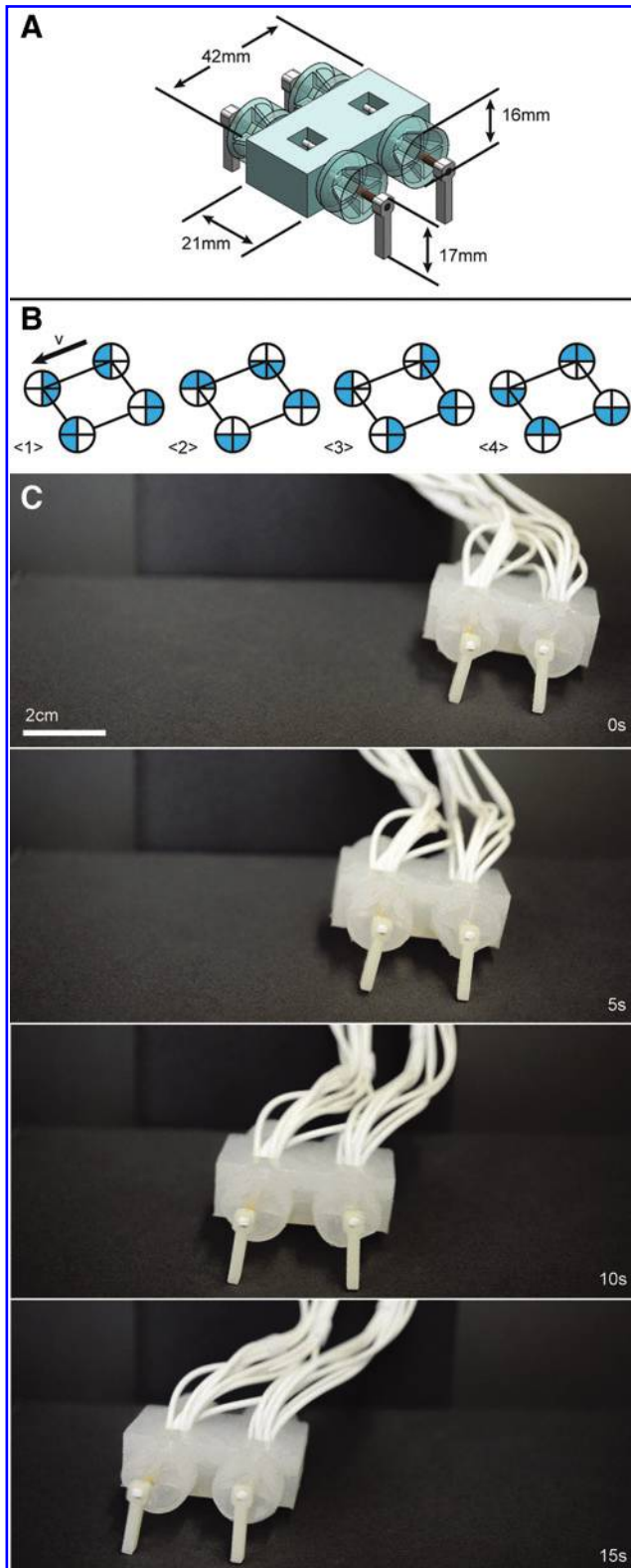
FIG. 6. Demonstration of locomotion with cVAMs. **(A)** A four-legged ''walker'' with four cVAMs to move its legs. **(B)** Vacuum pulses are applied to four chambers on each leg in a cyclic sequence. A phase difference of 180° exists between the front and back legs of each side, whereas two diagonal pairs of legs each have the same phase. **(C)** The ''walker'' moves at 0.5 cm/s (or 0.12 body length per second) when vacuum states are changed every 0.1 s.

Using the viscous drag force exerted by the fluids, we calculated the power output of the actuator as a function of frequency of revolution (Fig. 4F, details of calculations are given in the Supplementary Data). For the different frequencies of revolution, the work done per revolution by the actuator on the fluid remains approximately constant (because the force and displacement are the same for each step for the different frequencies of revolution).

As the frequency of revolution increases, the time period over which this work is done decreases, and hence the power dissipated while stirring increases. As expected, frequency of revolution and power are linearly related (Fig. 4F). The only exception is when the hold time (10 ms, with frequency of revolution of 750 rpm) for each step is shorter than the time interval required for the actuator to respond. In this regime, incomplete actuation leads to a decrease in the dissipated power.

Supplementary Figures S2 and S3 characterize the performance of the actuator when a load is applied at one end of the rod. These characteristics can be used to estimate the spring constant at $0.0095\,\mathrm{N\cdot m\cdot rad^{-1}}$, which is about double compared with the previous estimate ($0.0045\,\mathrm{N\cdot m\cdot rad^{-1}}$). In addition, the thermodynamic efficiency is $\sim 2\%$ and the power dissipated is about 2.3 mW (see Supplementary Data for details on calculations; for comparison, we have reported a soft linear actuator showing efficiency of $\sim 27\%$,[20] and biological muscles have efficiency of about 20–40%[30,31]). These characteristics could be improved by optimizing the design of the actuator, for example, by making the external walls thicker to minimize losses of energy by compression of the actuator.

Using cVAMs for delivering fluid while stirring

We replaced the central wooden dowel with a stainless steel needle (16G, 10 cm) and connected the needle to a tube (Tygon® S3) for delivering fluids. We attached a spherical ball at the base of the needle (see Supplementary Movie S2 for a demonstration of stirring) for two reasons: (1) to increase the drag force in viscous fluid and hence, the stirring ability and (2) to aid in characterization because a spherical shape simplifies force calculations (as discussed in the previous section).

Since the cVAMs produce a cyclical motion without rotating the needle, it is possible to deliver fluids without entangling the tubes. Using fluorescein (1 mM in water) as a model dye, we demonstrated that the cVAMs can be used to deliver fluid (at the rate of 10 mL/min) into a water bath (150 mL) while stirring at 375 rpm (hold time of 20 ms). Qualitatively, Figure 5 and Supplementary Movie S4 show that stirring using cVAMs can achieve a homogeneous solution (i.e., fluorescein is dispersed throughout the water bath) within 10 s while delivering fluorescein continuously. On the contrary, when the cVAM is not stirring, the delivery of fluorescein is heterogeneous even after 20 s (i.e., the convection created by stirring by cVAM is considerably more effective for mixing than diffusion alone, Fig. 5).

Using cVAMs for locomotion

Actuating the ring of pneumatic chambers in clockwise or counter-clockwise sequence causes the tip of the central rod to move in a cyclical manner while following an

approximately square trajectory (Fig. 3). We took advantage of this motion to build a quadrupedal soft robot that uses this cyclical movement to walk (Fig. 6). In designing a gait, we mimicked the walking gait of a reptile. While walking, a reptile moves its diagonal limbs simultaneously (Supplementary Fig. S11[32]) and so does our soft robot (Supplementary Movies S5–S7).

Conclusions

cVAMs offer a new method to generate a cyclical motion using a soft actuator. It is useful to compare the cVAM with the related device described by Mazzeo and colleagues.[22] Four advantages can be listed. (1) The cVAMs do not require a lubricant. (2) They cannot burst at actuation pressures more than their operating specifications because they operate under negative pressure (partial vacuum) rather than positive pressure. (3) The frequency of revolution is controlled by the hold time between steps while the negative pressure (in the chambers) controls the shape of the trajectory; Mazzeo's rotational actuator requires a critical pressure less than which there is no rotation because the inflation of the chambers depends on the pressure applied (and if the pressure is too low, the sequential inflation of chambers does not lead to rotation). This relationship allows us to achieve rapid revolutions (~ 750 rpm without altering the trajectory) compared with that in the actuator by Mazzeo *et al.* (~ 20 rpm at a comparable pressure difference of 90 kPa). (4) cVAMs contract rather than expand when being used, and thus can be used in space-constrained environments. The elastomers are less strained when operated using reduced pressure relative to operation under positive pressure and thus can have increased lifetime (we tested cVAMs with 10^6 cycles and the actuation remained unchanged, as seen in Supplementary Fig. S12).

cVAMs exhibit three limitations. (1) Under ambient conditions, the pressure difference is limited to ~ 100 kPa because cVAMs actuate using vacuum. This property governs the force that can be applied by the cVAMs. The limitation might become an advantage in hyperbaric conditions such as in deep-sea applications. (2) Operation of the cVAM involves many cycles of low amplitude stretching and compressing of the elastomer "hub," and failure in this region is a possibility (although unlikely for at least a million cycles, as seen in Supplementary Fig. S12). (3) cVAMs are not directly suitable for causing an axle and wheel to rotate because the central rod does not actually rotate, instead it follows an approximately square trajectory. Table 1 summarizes additional technical differences.

The cVAMs can be used to deliver fluids, or to sample, while stirring without entangling the tubes used for delivery (or sampling) as demonstrated by the stirring of fluorescein in Figure 5. Since the actuators are pneumatic, cVAMs can be used in operations that are sensitive to electromagnetic fields, or use flammable liquids, wherein unshielded electric motors could cause interference or explosion.

These cVAMs can be coupled to each other to mimic some parts of the motion used by animals (reptiles) to move their limbs in walking. In reptilian walking, several joints function together in each step. One characteristic of this gait is that diagonal limbs move simultaneously (or almost simultaneously)[32]; we implemented this diagonal co-ordination in our crude biomimetic model.

Authors' Contributions

A.A., M.S.V., D.Y., and G.M.W. designed the experiments. A.A. and D.Y. executed the experiments. D.Y. designed and fabricated the actuators. A.A. and D.Y. designed and fabricated the quadrupedal robots. M.S.V., D.Y., and A.A. analyzed the results. M.S.V., A.A., D.Y., and G.M.W. wrote the article.

Author Disclosure Statement

No competing financial interests exist.

References

1. Suzumori K, Iikura S, Tanaka H. Development of flexible microactuator and its applications to robotic mechanisms. In: Proceedings 1991 IEEE International Conference on Robotics and Automation, Sacramento, CA, 1991, pp. 1622–1627.
2. Suzumori K, Iikura S, Tanaka H. Flexible microactuator for miniature robots. In: 1991 Proceedings IEEE Micro Electro Mechanical Systems, Nara, Japan, 1991, pp. 204–209.
3. Ilievski F, Mazzeo AD, Shepherd RF, Chen X, Whitesides GM. Soft robotics for chemists. Angew Chem Int Ed Engl 2011; 50:1890–1895.
4. Martinez RV, Branch JL, Fish CR, Jin L, Shepherd RF, Nunes RM, *et al*. Robotic tentacles with three-dimensional mobility based on flexible elastomers. Adv Mater 2013;25: 205–212.
5. Mosadegh B, Polygerinos P, Keplinger C, Wennstedt S, Shepherd RF, Gupta U, *et al*. Pneumatic networks for soft robotics that actuate rapidly. Adv Funct Mater 2014;24:2163–2170.
6. Rus D, Tolley MT. Design, fabrication and control of soft robots. Nature 2015;521:467–475.
7. Trivedi D, Rahn CD, Kier WM, Walker ID. Soft robotics: biological inspiration, state of the art, and future research. Appl Bionics Biomech 2008;5:99–117.
8. Pfeifer R, Lungarella M, Iida F. The challenges ahead for bio-inspired 'soft' robotics. Commun ACM 2012;55:76–87.
9. Kim S, Laschi C, Trimmer B. Soft robotics: a bioinspired evolution in robotics. Trends Biotechnol 2013;31:23–30.
10. Trimmer B. Soft robots. Curr Biol 2013;23:R639–R641.
11. Bauer S, Bauer-Gogonea S, Graz I, Kaltenbrunner M, Keplinger C, Schwodiauer R. 25th Anniversary article: a soft future: from robots and sensor skin to energy harvesters. Adv Mater 2014;26:149–162.
12. Majidi C. Soft robotics: a perspective-current trends and prospects for the future. Soft Robot 2014;1:5–11.

13. Laschi C, Cianchetti M. Soft robotics: new perspectives for robot bodyware and control. Front Bioeng Biotechnol 2014;2:1–5.

14. Lu NS, Kim DH. Flexible and stretchable electronics paving the way for soft robotics. Soft Robot 2014;1:53–62.

15. Jaeger HM. Celebrating soft matter's 10th anniversary: toward jamming by design. Soft Matter 2015;11:12–27.

16. Marchese AD, Katzschmann RK, Rus D. A recipe for soft fluidic elastomer robots. Soft Robot 2015;2:7–25.

17. Whitesides GM. Bioinspiration: something for everyone. Interface Focus 2015;5:1–10.

18. Hughes J, Culha U, Giardina F, Guenther F, Rosendo A, Iida F. Soft manipulators and grippers: a review. Front Robot AI 2016;3:1–12.

19. Zolfagharian A, Kouzani AZ, Khoo SY, Moghadam AAA, Gibson I, Kaynak A. Evolution of 3D printed soft actuators. Sensor Actuat A Phys 2016;250:258–272.

20. Yang D, Verma MS, So J-H, Mosadegh B, Keplinger C, Lee B, et al. Buckling pneumatic linear actuators inspired by muscle. Adv Mater Technol 2016;1:1600055.

21. Yang D, Verma MS, Lossner E, Stothers D, Whitesides GM. Negative-pressure soft linear actuator with a mechanical advantage. Adv Mater Technol 2016;2:1600164.

22. Gong X, Yang K, Xie J, Wang Y, Kulkarni P, Hobbs AS, et al. Rotary actuators based on pneumatically driven elastomeric structures. Adv Mater 2016;28:7533–7538.

23. Wait KW, Jackson PJ, Smoot LS. Self locomotion of a spherical rolling robot using a novel deformable pneumatic method. In: IEEE International Conference on Robotics, Anchorage, AK, 2010, pp. 3757–3762.

24. Marchese AD, Onal CD, Rus D. Soft robot actuators using energy-efficient valves controlled by electropermanent magnets. In: 2011 IEEE/RSJ International Conference on Intelligent Robots and System (IROS), San Francisco, CA, 2011, pp. 756–761.

25. Mazzolai B, Margheri L, Cianchetti M, Dario P, Laschi C. Soft-robotic arm inspired by the octopus: II. From artificial requirements to innovative technological solutions. Bioinspir Biomim 2012;7:025005.

26. Correll N, Önal ÇD, Liang H, Schoenfeld E, Rus D. Soft Autonomous Materials—Using Active Elasticity and Embedded Distributed Computation (Experimental Robotics: The 12th International Symposium on Experimental Robotics). Berlin, Heidelberg: Springer Berlin Heidelberg, 2014.

27. Morin SA, Kwok SW, Lessing J, Ting J, Shepherd RF, Stokes AA, et al. Elastomeric tiles for the fabrication of inflatable structures. Adv Funct Mater 2014;24:5541–5549.

28. Morin SA, Shevchenko Y, Lessing J, Kwok SW, Shepherd RF, Stokes AA, et al. Using "click-E-bricks" to make 3d elastomeric structures. Adv Mater 2014;26:5991–5999.

29. Lazarus A, Reis PM. Soft actuation of structured cylinders through auxetic behavior. Adv Eng Mater 2015;17:815–820.

30. Madden JDW, Vandesteeg NA, Anquetil PA, Madden PGA, Takshi A, Pytel RZ, et al. Artificial muscle technology: physical principles and naval prospects. IEEE J Oceanic Eng 2004;29:706–728.

31. Huber JE, Fleck NA, Ashby MF. The selection of mechanical actuators based on performance indices. Proc R Soc Lond A 1997;453:2185–2205.

32. Reilly SM, Delancey MJ. Sprawling locomotion in the lizard sceloporus clarkii: quantitative kinematics of a walking trot. J Exp Biol 1997; 200:753–765.

Address correspondence to:
George M. Whitesides
Department of Chemistry and Chemical Biology
Harvard University
12 Oxford Street
Cambridge, MA 02138

E-mail: gwhitesides@gmwgroup.harvard.edu